



Selective Aberrant Functional–Structural Coupling of Multiscale Brain Networks in Subcortical Vascular Mild Cognitive Impairment

Juanwei Ma¹ · Feng Liu¹ · Bingbing Yang¹ · Kaizhong Xue¹ · Pinxiao Wang¹ · Jian Zhou¹ · Yang Wang¹ · Yali Niu² · Jing Zhang¹

Received: 13 January 2020 / Accepted: 30 May 2020 / Published online: 25 September 2020
© Shanghai Institutes for Biological Sciences, CAS 2020

Abstract Subcortical vascular mild cognitive impairment (svMCI) is a common prodromal stage of vascular dementia. Although mounting evidence has suggested abnormalities in several single brain network metrics, few studies have explored the consistency between functional and structural connectivity networks in svMCI. Here, we constructed such networks using resting-state fMRI for functional connectivity and diffusion tensor imaging for structural connectivity in 30 patients with svMCI and 30 normal controls. The functional networks were then parcellated into topological modules, corresponding to several well-defined functional domains. The coupling between the functional and structural networks was finally estimated and compared at the multiscale network level (whole brain and modular level). We found no significant intergroup differences in the functional–structural coupling within the whole brain; however, there was significantly increased functional–structural coupling within the dorsal attention module and decreased functional–structural coupling within the ventral attention module in the svMCI group. In addition, the svMCI patients demonstrated decreased intramodular connectivity strength in the visual,

somatomotor, and dorsal attention modules as well as decreased intermodular connectivity strength between several modules in the functional network, mainly linking the visual, somatomotor, dorsal attention, ventral attention, and frontoparietal control modules. There was no significant correlation between the altered module-level functional–structural coupling and cognitive performance in patients with svMCI. These findings demonstrate for the first time that svMCI is reflected in a selective aberrant topological organization in multiscale brain networks and may improve our understanding of the pathophysiological mechanisms underlying svMCI.

Keywords Resting-state fMRI · Diffusion tensor imaging · Functional–structural coupling · Modular architecture · Subcortical vascular mild cognitive impairment

Introduction

Vascular cognitive impairment (VCI) refers to all levels of cognitive loss attributable to cerebrovascular diseases with a range of cognitive deficits from mild cognitive decline to broad dementia [1]. There are three VCI subtypes: VCI-no dementia, vascular dementia (VaD), and mixed dementia (usually Alzheimer’s disease with vascular dementia) [2]. VaD is the second most common cause of dementia after Alzheimer’s disease [1, 3]. VCI-no dementia, also termed vascular mild cognitive impairment (vMCI), is regarded as a potentially transitional condition between normal aging and VaD [1]. Subcortical vMCI (svMCI) is characterized by multiple lacunar infarctions and extensive white matter hyperintensity in subcortical structures on MRI [4, 5]. Recently, svMCI has been attracting attention since it is potentially reversible [6, 7] as a prodromal stage of

Juanwei Ma, Feng Liu have contributed equally to this work.

Electronic supplementary material The online version of this article (<https://doi.org/10.1007/s12264-020-00580-w>) contains supplementary material, which is available to authorized users.

✉ Jing Zhang
zhangjing1970@163.com

¹ Department of Radiology and Tianjin Key Laboratory of Functional Imaging, Tianjin Medical University General Hospital, Tianjin 300052, China

² Department of Rehabilitation, Tianjin Medical University General Hospital, Tianjin 300052, China

subcortical VaD [4, 8, 9]. Therefore, characterizing the functional and structural abnormalities in svMCI may provide valuable information for delaying the transition from svMCI to VaD. Although some research has been carried out on svMCI during the last decade, its neuropathological mechanisms remain poorly understood.

A widely applicable method of assessing relationships in data, graph theory has been frequently used to measure both the structural and functional connectivity in brain imaging data [10]. Graph-based network analysis allows the interpretation of neural activity in the brain and sheds light on potential physiological or disease processes from the network and information-processing viewpoints [11–13]. Indeed, recent neuroscientific investigations have shown alterations in brain network topologies in VCI, especially in svMCI patients. For instance, subcortical VCI, one of its most common subtypes [12], has been shown to exhibit widely reduced global efficiency and clustering coefficients and increased characteristic path lengths in functional networks. Furthermore, the clustering coefficient and global efficiency have been found to be closely correlated with cognitive performance in subcortical VCI [14]. In addition, in one study of 21 svMCI patients and 26 healthy controls, Yi *et al.* found disrupted global functional network topology with significantly increased modularity, path length, and intermodular connectivity in the inferior and superior parietal lobule in the patient group. In addition, increased intermodular connectivity was associated with worse cognitive performance in patients [15]. In addition to the abnormal functional network properties, patients with VCI also exhibit altered structural network parameters. Specifically, Jang *et al.* reported more severe structural network disruptions such as decreased mean nodal strength in the frontal area and frontal-executive dysfunction in early-onset than in late-onset subcortical VCI patients [16]. Moreover, recent studies have revealed that such alterations are not restricted to the global network architecture in VCI. For example, Sang and colleagues reported that both local and global efficiency progressively decreased as cognitive impairment worsened in the functional networks of patients with subcortical ischemic VCI [17]. However, these studies mainly focused on single network properties. The interaction between the human functional and structural networks in svMCI has not yet been fully investigated. The human brain has been modeled as a large-scale integrated complex network in the functional and structural domains [18]. It is increasingly recognized that structural connectivity places anatomical constraints on functional connectivity in the network [19], and in turn, functional connectivity has an effect on structural connectivity through brain plasticity [20, 21]. Mapping the functional and structural connectivity would expand our understanding of how the functional–

structural (F–S) relationship underlies human cognition and behavior [22]. Thus, exploration of F–S associations at the network level may provide deeper insight into the mechanism underlying svMCI.

F–S coupling, an emerging integrative measure associating the functional with the structural network, has been recognized as a more sensitive modality for detecting subtle changes in brain activity than any single-modality index [18]. In recent years, it has been suggested that large-scale networks may play a critical role in the establishment of F–S associations [22]. Specifically, disrupted F–S coupling in large-scale networks have been revealed in several neuropsychiatric disorders, such as schizophrenia [23], idiopathic generalized epilepsy [18], and psychogenic non-epileptic seizures [24]. Since the human brain is a complex network that is functionally segregated and integrated simultaneously via specific connectivity patterns, it may not be enough to only investigate the large-scale (whole brain) F–S coupling. Recently, regional decreased F–S coupling has also been reported, such as in the fronto-striatal, fronto-temporal, and fronto-thalamic regions [25], the hippocampus, and the caudate [25, 26]. These studies are helpful for deepening our understanding of the F–S relationship in specific functionally-segregated domains.

Functional segregation involves neuronal processing carried out among regions within modules [27]. The modular structure of human brain networks is topologically composed of a group of interconnected nodes, characterized by local integration within them for specialized functions [28]. Despite their quantity and varied distribution, functionally-coupled modules contribute to the balance of functional segregation and integration while conserving wiring length [29], efficient intramodular information processing [29, 30], rapid intermodular information exchange [31], and high resilience to network node or edge failure [32, 33]. Human functional brain networks contain well-defined modular organizations corresponding to many well-known functions [34], such as the somatosensory/motor, auditory, attention, visual, subcortical, and default-mode systems. It has been thought that svMCI patients exhibit cognitive impairments in executive, language, visuospatial, and memory functions [4, 8, 35, 36]; therefore, further investigations into the alterations in F–S coupling at the functional modular level may advance our knowledge of the neuropathological underpinnings of this disorder.

On the basis of previous work, we examined how F–S coupling changes in svMCI for multiscale networks: first, we tested whether whole-brain F–S coupling showed any changes; second, we investigated whether the modular organization overlapping with functional domains exhibited abnormal F–S coupling and, if so, whether disease–

related alterations were correlated with cognitive impairment. Based upon the results of widespread topological disruption of functional and structural connectivity networks across the whole brain [14, 37] and cognitive impairments in specialized functions [8, 35, 36], we hypothesized that F–S coupling is affected at the multiscale network level (whole brain and modular level) in svMCI. The present findings may provide important insights into the early-phase identification of svMCI and the prevention of the transition from svMCI to dementia.

Materials and Methods

Participants

The study was approved by the Research Ethics Committee of Tianjin Medical University General Hospital, and written informed consent was given all participants. A total of 64 participants were enrolled from Tianjin Medical University General Hospital: 33 patients with svMCI and 31 gender-, age- and education-matched normal controls (NCs). All patients and NCs were subjected to the Montreal Cognitive Assessment (MoCA) to evaluate their cognitive function.

All patients met the inclusion criteria [17, 38]: (1) age between 50 and 75 years; (2) subjective cognitive decline reported by his/her caregivers; (3) cognitive impairment with MoCA score < 26 ; (4) history of clinical ischemic stroke with an anatomically corresponding subcortical infarct < 1.5 cm in diameter on MRI; (5) time from stroke onset ≥ 3 months; (6) insufficient cognitive decline to fulfill the DSM-V criteria for dementia; (7) Hachinski Ischemic Score ≥ 7 ; and (8) willingness to undergo MRI and neuropsychological examinations. The exclusion criteria were as follows: (1) pre-existing cognitive impairment prior to stroke; (2) cognitive impairment due to head trauma or other psychiatric disorders; (3) acute-phase cerebrovascular disease; (4) alcoholism or drug abuse; and (5) severe contraindications to MRI.

Thirty-one healthy volunteers matched for gender, age, and years of education participated in this study. All enrolled NCs had normal cognitive function and had no known neurological or psychotic disorders. Individuals who had any history of neurological illness, psychiatric illness, systemic disease, major medical conditions, substance/alcohol abuse, or other MRI contraindications (e.g., claustrophobia) were excluded. All participants underwent neuroimaging scans, and brain MRI images were visually checked by two experienced neuroradiologists to ensure image quality.

Data Acquisition

MRI data were obtained using a 3T Siemens Prisma MR scanner equipped with a 64-channel head coil at Tianjin Medical University General Hospital. Foam padding and earplugs were used to minimize head movement and scanner noise. During the scan, all participants were instructed to remain motionless, keep their eyes closed, and think of nothing. Sagittal high-resolution three-dimensional T1-weighted images were collected using a magnetization-prepared rapid gradient-echo sequence: repetition time (TR)/echo time (TE) = 2000/2.26 ms; inversion time = 900 ms; field of view (FOV) = 256×256 mm²; matrix size = 256×256 ; flip angle = 8°; slice thickness = 1 mm; voxel size = $1 \times 1 \times 1$ mm³, and 192 sagittal slices without interslice gaps. Resting-state functional images were obtained using a single-shot echo-planar-imaging (SS-EPI) sequence: TR/TE = 750/30 ms; FOV = 222×222 mm²; matrix size = 74×74 ; flip angle = 54°; slice thickness = 3 mm; voxel size = $3 \times 3 \times 3$ mm³; 48 transverse slices; and 640 volumes. Diffusion tensor images were also acquired using an SS-EPI sequence: TR/TE = 2500/70 ms; FOV = 256×256 mm²; flip angle = 90°; slice thickness = 2 mm; matrix size = 128×128 ; voxel size = $2 \times 2 \times 2$ mm³; 68 transverse slices; 64 noncollinear directions ($b = 1000$ s/mm²), and 1 b0 ($b = 0$ s/mm²) images. To increase the signal-to-noise ratio, the entire sequence was repeated twice using posterior-to-anterior and anterior-to-posterior phase-encoding directions.

Brain Parcellation

Graph-theoretical analysis demonstrates that brain networks are comprised of nodes and edges. To determine the nodes of functional and structural networks, the whole cerebral cortex was divided into 300 functionally homogeneous nodes according to the Schaefer-300 template [39]. This template was defined by the similarity of global functional connectivity and local functional connectivity gradients and has been widely used in previous studies, revealing physically meaningful features of brain organization and superior functional and connective homogeneity relative to other parcellations [39, 40]. The processing flowchart is depicted in Fig. 1.

Identification of Brain Network Modules

To examine the module-level impact of F–S coupling and evaluate between-group differences, we used the canonical 7-network parcellation given by Yeo *et al.* [41] to define functional modules and assigned each node from the Schaefer-300 template to one of the 7 modules [39, 41]: the

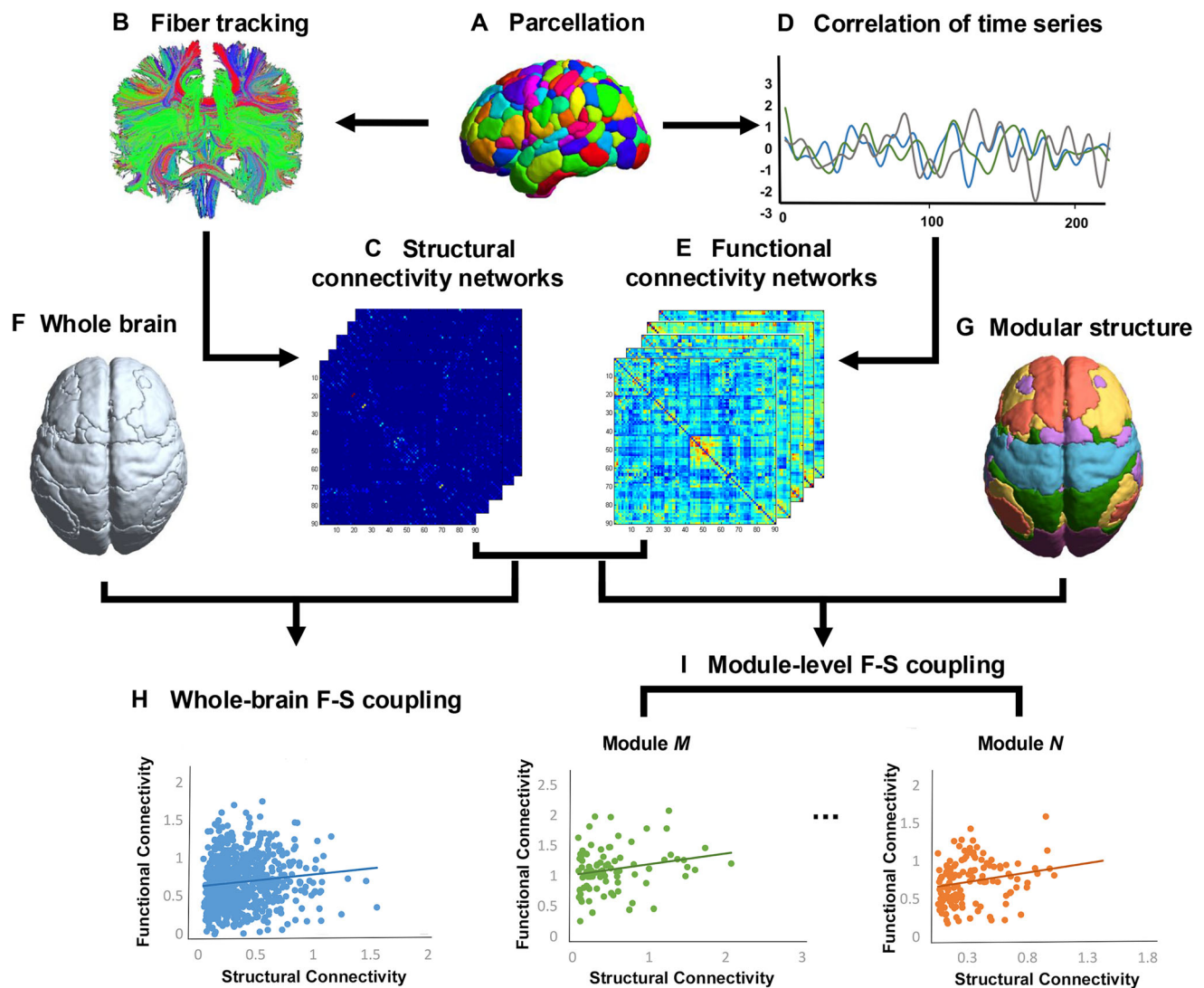


Fig. 1 Flowchart of data analysis. **A** Schaefer-300 parcellation for both structural and functional connectivity network construction. **B** Whole-brain deterministic fiber tracking in native diffusion space. **C** Computation of the individual structural connectivity matrices. **D** Pearson correlations of the mean time series in each region.

E Computation of the individual functional connectivity matrices. **F** Whole brain. **G** Seven functional modular structures defined by Yeo *et al.* [41]. **H** Whole-brain F–S coupling analysis within the whole brain. **I** Module-level F–S coupling within the modular structures. F–S coupling, functional-structural coupling.

visual, somatomotor, dorsal attention, ventral attention, limbic, and frontoparietal control modules, and the default mode network (Figs 2 and S1). The region labels and corresponding modules in the Schaefer-300 template are shown in Table S1.

Functional Connectivity Network Construction

The resting-state fMRI pre-processed via Statistical Parametric Mapping (SPM12, <http://www.fil.ion.ucl.ac.uk/spm>) and Data Processing Assistant for Resting-State fMRI (DPARSF, <http://www.restfmri.net>) software. First, head motion was corrected between time points. Subsequently, each participant's T1 images were co-registered to the

mean functional images and segmented into gray matter, white matter, and cerebrospinal fluid. In addition, nuisance covariate regressions were performed (including 24 motion parameters, white matter, and cerebrospinal fluid signals). Then, temporal bandpass filtering (0.01–0.1 Hz) was implemented. Finally, these images were warped into the standard Montreal Neurological Institute (MNI) space and resampled to $3 \times 3 \times 3 \text{ mm}^3$ voxel resolution. Of note, normalized images were not spatially smoothed to avoid artificial spatial correlations [42, 43]. As noted above, the nodes in the functional connectivity network construction represented the 300 regions parcellated according to the Schaefer-300 template. The edges were defined as the Pearson correlation coefficient between the mean time

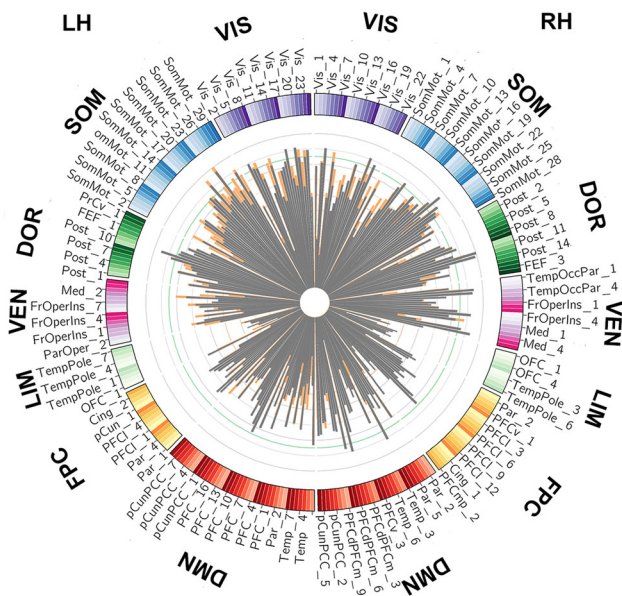


Fig. 2 Brain regions belonging to each module in the left and right hemispheres. The concentric gray and orange histograms represent the mean intramodular functional connectivity strength of each region within each module in the svMCI and NC groups, respectively. DMN, default mode network; DOR, dorsal attention module; FPC, frontoparietal control module; LIM, limbic module; LH, left hemisphere; NC, normal control; RH, right hemisphere; SOM, somatomotor module; svMCI, subcortical vascular mild cognitive impairment; VEN, ventral attention module; VIS, visual module.

series of each node to generate a whole-brain functional network. Consistent with previous studies [44–47], negative correlations in the functional connectivity network were excluded from this study due to their ambiguous physiological interpretation.

Structural Connectivity Network Construction

Diffusion images were processed with FSL (<https://fsl.fmrib.ox.ac.uk/fsl/fslwiki>) and Diffusion Toolkit (<http://www.trackvis.org/dtk>) software with the following steps. First, eddy current and movement-related distortion was corrected using the b0 image as a reference. Second, a binary brain mask was generated from the b0 image. Third, diffusion tensor models were fitted independently for each voxel using the linear least-squares method within the binary mask. Finally, whole-brain fiber tracking was performed in native diffusion space using the fiber assignment by a continuous tracking algorithm [48]. Tracts were traced at the center of the voxels until fractional anisotropy values were ≤ 0.15 , the tract turning angle was $\geq 45^\circ$, or the fiber tracks left the mask, as suggested in previous studies [49–51].

To construct structural connectivity networks for each participant, the skull-stripped T1-weight images were first

linearly co-registered to their b0 images in the native diffusion space by applying the FSL linear registration tool. These co-registered images were then transformed to MNI space. The resulting transformation parameters were inverted to map the Schaefer-300 image from MNI space to the native diffusion tensor space, which has been applied extensively in previous studies [52, 53]. To reduce the impact of noise-related pseudo-connections, between-region connectivity was considered to be established when at least three fiber tracts were traced between both regions [26]. The density of streamlines (number of streamlines per unit surface) was defined as an edge between a pair of regions for each participant to correct for the different surface sizes of regions [54].

Whole-Brain and Module-Level F–S Coupling

We extracted all non-zero elements from the structural matrix for each participant, as previously described [18], to predict functional connectivity from the structural networks [19]. Subsequently, to evaluate the coupling between the top strong structural and functional connectivities, we used a sparsity-based thresholding approach. Specifically, sparsity was defined as the percentage of the number of actual connections out of the number of possible connections within a network [42, 55, 56]. We selected a threshold of sparsity of 50% on the group-level mean functional network within each group as the top strong connectivities, resulting in a set of connections with the strongest functional connections. Whole-brain and module-level F–S coupling were analyzed on these connections, where we could capture the strongest connectivity while maintaining the network backbone. Unless stated otherwise, we report our results at this threshold. Given that different sparsities would have an effect on the F–S coupling, we also evaluated the coupling by applying a sparsity threshold of 30% to re-define the top strong functional connectivities. In addition, F–S coupling was calculated using Spearman rank correlation between the functional connectivity and its non-zero structural connectivity counterparts for these connections at the whole brain level (correlations across the whole brain) and each modular level (correlations within a module) [57–59].

Intramodular and Intermodular Connectivity Strength

Intramodular connectivity strength is an evaluation index for the significance of a particular module within the brain network, which is calculated as the mean of all connective weights within the module. The intermodular connectivity strength between two modules is the mean of the connective weights connecting both modules. In

the current study, the intramodular and intermodular connectivity strengths in the functional connectivity and structural connectivity networks were calculated.

Statistical Analysis

Participant characteristics, including gender, age, years of education and cognitive performance (MoCA scores), were compared between groups. χ^2 tests were used for categorical variables and independent samples *t*-tests for continuous variables. Nonparametric permutation testing was used to assess the between-group differences in whole-brain and modular F–S coupling, and intramodular and intermodular connectivity strength. First, for a given measure, the real mean differences between groups were calculated. Second, all participants were randomly re-assigned to each group with the number of participants in each group unchanged, the measure calculation was repeated and the permuted mean differences between groups was calculated. Repeating the permutation process 10000 times, we counted the number of permutations in which the permuted mean differences of the given measure was higher than the real mean difference [43]. Third, after dividing by the total number of permutations, the *P*-value was acquired. Multiple comparisons were corrected using the false discovery rate (FDR) method. Moreover, we explored whether altered F–S coupling was associated with decreased cognitive function. To this end, multiple linear regressions were performed with gender, age, and years of education as confounding variables.

Results

Demographics and Clinical Characteristics of the Participants

Four participants (three patients and one healthy control) were excluded due to excessive motion, defined as greater than ± 2 mm of translational movement or $\pm 2^\circ$ of rotational movement. Table 1 shows the demographic and

clinical characteristics for the svMCI patients and NCs. The results did not show any significant differences between the two groups in age ($P = 0.740$), gender ($P = 0.301$), or years of education ($P = 0.431$). However, the svMCI group had significantly lower MoCA scores than the NC group ($P < 0.001$).

Preserved Whole-Brain F–S Coupling in Patients with svMCI

Under the constraint of non-zero structural connections, correlation analysis was performed between functional connections and their structural counterparts in the whole-brain network across participants. The whole-brain functional connectivities were positively correlated with the structural connection values, consistent with previous studies [19, 26]. F–S coupling was preserved across the whole brain in the patient group. Specifically, the strength of the whole-brain F–S coupling did not differ significantly between groups (NC vs svMCI: 0.1043 ± 0.0485 (range, 0.0144–0.1977) vs 0.1118 ± 0.0505 (range, 0.0026–0.2008), $P = 0.5894$, FDR corrected, 10000 permutations) (Fig. 3). Similarly, there was no significant difference in the whole-brain F–S coupling when applying the sparsity threshold of 30% (NC vs svMCI: 0.0819 ± 0.0517 (range, 0.0143–0.1892) vs 0.0962 ± 0.0484 (range, 0.0076–0.1689), $P = 0.2771$, FDR corrected, 10000 permutations) (Fig. S2).

Disrupted Modular F–S coupling in Patients with svMCI

The module-level analysis revealed that the changes in F–S coupling were different within each module in the svMCI group. Compared with the NCs, the svMCI group showed significantly increased F–S coupling in the dorsal attention module ($P = 0.0308$, FDR corrected, 10000 permutations). In addition, a significant decrease in F–S coupling was found in the ventral attention module ($P = 0.0364$, FDR corrected, 10000 permutations) for patients with svMCI (Fig. 3). In addition, altered module-level F–S coupling in

Table 1 Demographics and clinical characteristics of the participants.

Characteristics	svMCI (<i>n</i> = 30)	NCs (<i>n</i> = 30)	Statistics (<i>t</i> or χ^2)	<i>P</i> value
Age (years)	58.57 (52–72)	58.07 (50–72)	<i>t</i> = 0.333	0.740
Gender (F/M)	14/16	18/12	χ^2 = 1.071	0.301
Education (years)	11.3 (0–16)	12.1 (0–16)	<i>t</i> = 0.793	0.431
MoCA score	21.8 (18–25)	27.5 (26–30)	<i>t</i> = 11.079	< 0.001

Both the mean and range (minimum to maximum values) are shown.

F female, M male, MoCA Montreal Cognitive Assessment, NCs normal controls, svMCI subcortical vascular mild cognitive impairment.

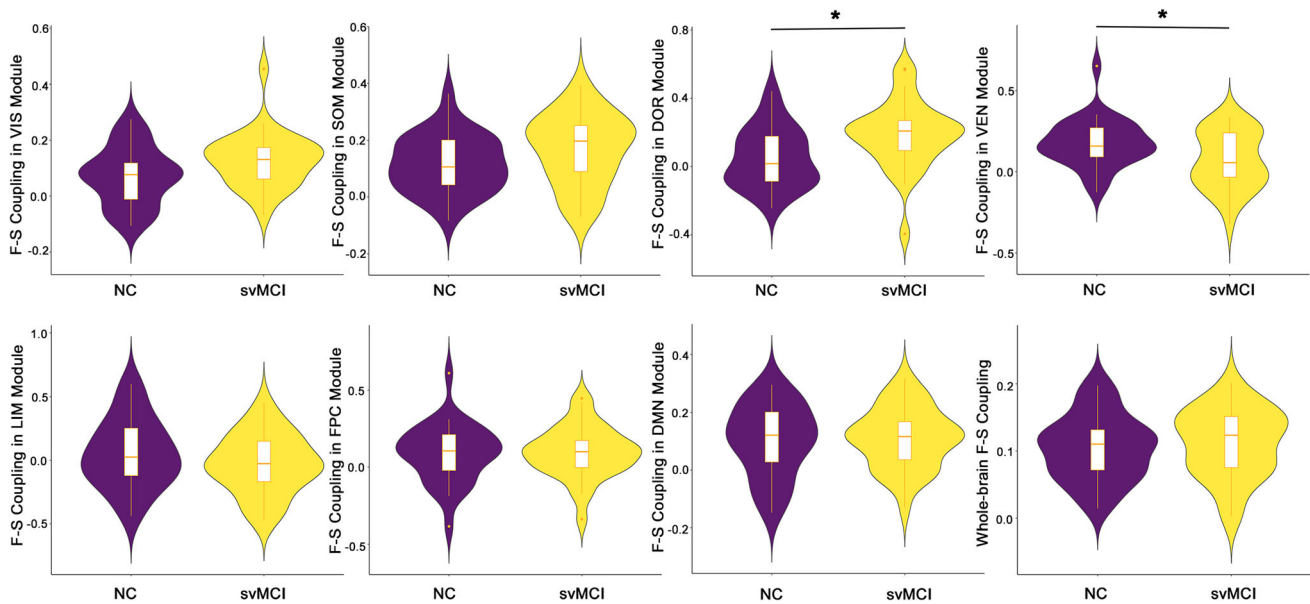


Fig. 3 Multiscale F–S coupling analysis. Patients with svMCI had significantly increased F–S coupling in the dorsal attention module ($P = 0.0308$, FDR corrected) but decreased F–S coupling in the ventral attention module ($P = 0.0364$, FDR corrected). The whole-brain F–S coupling did not differ significantly between groups ($P = 0.5894$, FDR corrected). Violin plots extend the density distribution of F–S coupling. For the box plot inside the violin plots, the two endpoints of the vertical line indicate the maximum and minimum values, the

two ends of the rectangle indicate the first and third quartile values, and the horizontal line near the middle of the rectangle indicates the median of the F–S coupling. *FDR corrected $P < 0.05$. DMN, default mode network; DOR, dorsal attention; FDR, false discovery rate; FPC, frontoparietal control; F–S coupling, functional-structural coupling; LIM, limbic; SOM, somatomotor; VIS, visual; VEN, ventral attention.

the svMCI group was not significantly correlated with cognitive performance (MoCA scores). Consistent module-level F–S coupling changes were found when applying the 30% sparsity in defining the top strong functional connectivities (Fig. S2).

Altered Intramodular and Intermodular Connectivity Strengths

The mean intramodular functional connectivity strength of each region is presented in Fig. 2. Compared with the NCs, patients with svMCI showed a decrease in intramodular connectivity strength within the visual ($P = 0.0245$, FDR corrected, 10000 permutations), somatomotor ($P = 0.0347$, FDR corrected, 10000 permutations) and dorsal attention ($P = 0.0464$, FDR corrected, 10000 permutations) modules of the functional connectivity network (Fig. 4A). Furthermore, statistical analysis revealed that the svMCI patients showed decreased intermodular connectivity strength in 8 pairs of modules in the functional connectivity network (see Table S2 for details). In contrast, no significant difference in the intramodular and intermodular connectivity strength of the structural connectivity network was found between the groups (Fig. 4B).

Discussion

This is the first study investigating svMCI from the perspective of the association of F–S connections at the whole brain and modular levels. There were three main findings: (1) F–S coupling was preserved at the whole brain level, suggesting unbroken macroscopic network organization across the brains of svMCI patients; (2) at the modular level, significantly increased F–S coupling in the dorsal attention module and decreased F–S coupling in the ventral attention module in svMCI patients; and (3) svMCI patients demonstrated reduced intramodular connectivity strength in the visual, somatomotor, and dorsal attention modules and reduced intermodular connectivity strength between several modules of the functional connectivity network. The preserved whole-brain coupling and discrepant F–S coupling changes in both attention systems reflect disturbed segregation and integration of complex networks in patients with svMCI, providing avenues to better understand the pathophysiological mechanisms of svMCI.

In the present study, we investigated the multiscale F–S relations in the whole and modular brain networks in patients with svMCI. Patients and NCs showed a clear positive correlation between whole-brain functional and structural network correlation matrices, in accordance with

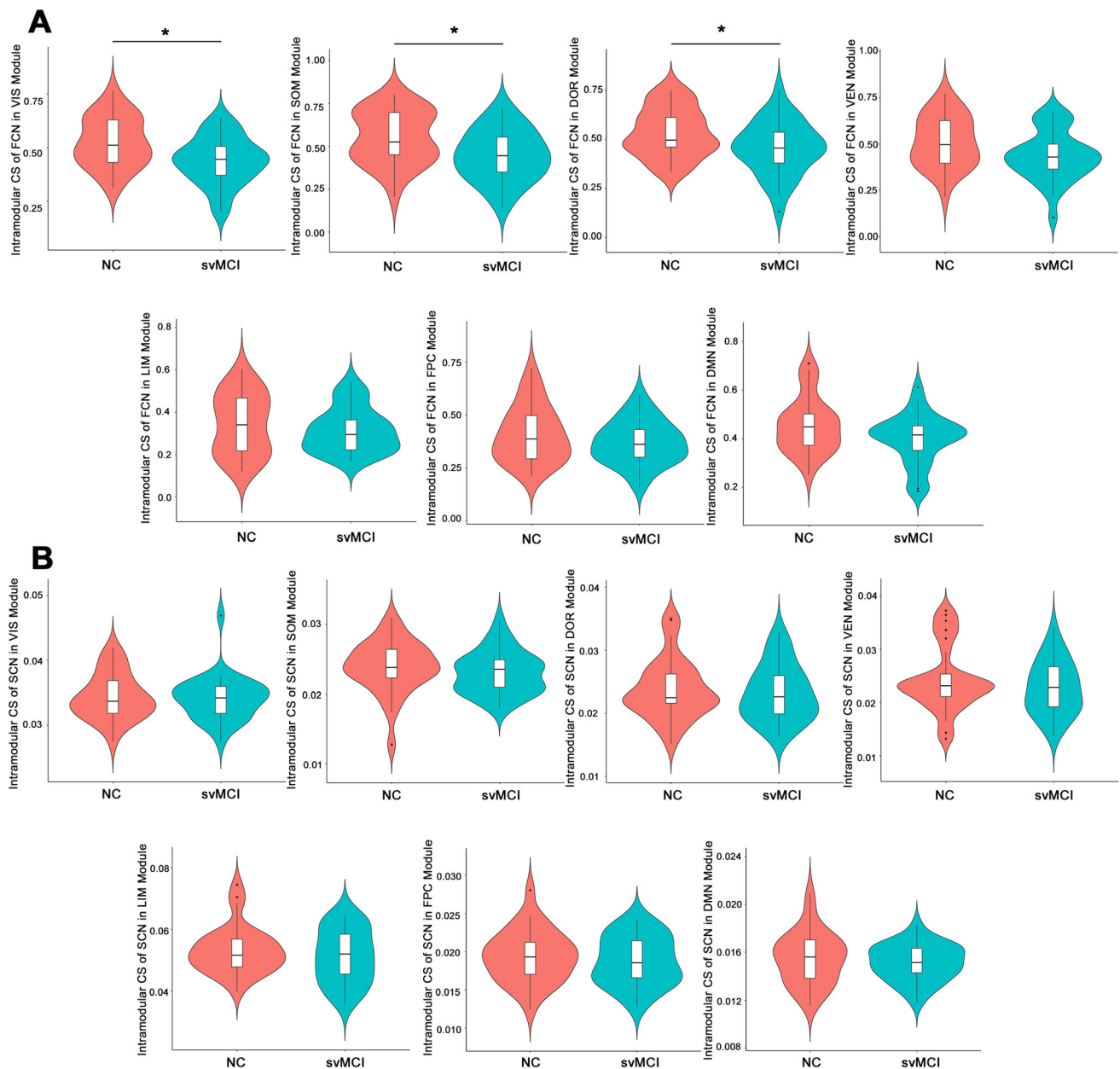


Fig. 4 Intramodular connectivity strength in the functional and structural connectivity networks. **A** Decreased intramodular connectivity strengths within the visual ($P = 0.0245$, FDR corrected), somatomotor ($P = 0.0347$, FDR corrected), and dorsal attention ($P = 0.0464$, FDR corrected) modules in the functional connectivity network in svMCI. **B** Intramodular connectivity strengths in the structural connectivity network does not significantly differ between groups. Violin plots show the distribution of intramodular connectivity strength and its probability density. For the box plot inside

violin plots, the top of the rectangle indicates the third quartile, the horizontal line near the middle of the rectangle indicates the median, and the bottom of the rectangle indicates the first quartile of intramodular connectivity strength. Its maximum and minimum values are marked by the two endpoints of the vertical line. *FDR corrected $P < 0.05$, CS, connectivity strength; FCN, functional connectivity network; FDR, false discovery rate; NC, normal control; SCN, structural connectivity network; svMCI, subcortical vascular mild cognitive impairment.

previous F–S coupling studies in large-scale brain networks [18, 20, 60]. Whole-brain F–S coupling did not show between-group differences, which suggests a globally intact F–S association in the brain integration of svMCI patients. In the present work, altered module-level F–S couplings were found in svMCI patients: specifically,

decreased F–S coupling in the ventral attention module and increased F–S coupling in the dorsal attention module, which suggest changes in consistency between the functional and structural connectivity networks within the two modules. The ventral attention module is involved in reorienting attention in response to salient sensory stimuli,

while the dorsal attention module is responsible for the endogenous attention-orienting process [61]. An impaired ventral attention module has been reported in patients with VCI in prior work [62, 63]. Our results are also largely consistent with a previous study showing that patients with svMCI exhibit greater activation within key structures in the dorsal attention module (inferior frontal gyrus and anterior inferior parietal lobule) [64], whereas those with VaD exhibit decreased activity in these regions. This finding suggests that the increased F–S coupling in the dorsal attention module in patients with svMCI may be compensatory. As noted above, whole-brain F–S coupling was preserved in svMCI patients. Hence, we concluded that module-dependent F–S coupling may have priority in capturing slight changes in neural activity in svMCI. Furthermore, significantly reduced intramodular connectivity strengths were shown in the visual, somatomotor, and dorsal attention modules, and reduced intermodular connectivities between several modules in the functional network, mainly linking the visual, somatomotor, dorsal attention, ventral attention, and frontoparietal control modules. The complex intramodular and intermodular functional disconnection with preserved structural connections might account for the aberrant module-level F–S couplings.

In the current study, module-level F–S couplings in the svMCI group were not significantly correlated with cognitive performance. There are several potential reasons for this result: (1) the changes in module-level F–S coupling in patients might be trait-like, enduring disruptions governing brain function and structure regardless of the severity of the cognitive impairment; (2) the module-level F–S couplings that define diagnosis may not be the abnormal measures that give rise to a more severe expression of cognitive decline; and (3) the relatively small sample size may yield low statistical power for the tests used to detect significant correlations.

Several limitations of the current study should be noted. First, we used static functional connectivity to estimate F–S coupling. Recently, a few studies have shown dynamic changes in functional connectivity at rest over time [65, 66] and F–S coupling alterations in the dynamic acute rising phase of functional connectivity [67]. Thus, further studies concerning dynamic F–S coupling over time in patients with svMCI are needed. Second, we used the Schaefer atlas to divide the whole cortex into 300 regions. However, different parcellation schemes may result in slight change in brain network organization and parameters [68, 69]. Whether other parcellation schemes would verify these findings should be explored. Third, we used a uniform canonical 7-network parcellation for all participants to facilitate comparisons between groups. However, recent precision mapping studies have suggested that functional

boundaries can systematically vary widely across individuals [70–73], which may exert an influence on individual F–S couplings [74]. As a result, the F–S couplings may not have been perfectly captured due to spatial variation or misaligned regions across individuals. Therefore, further studies integrating node annotations are needed.

Conclusions

In summary, the results of our multiscale F–S relationship study indicate selective aberrant F–S coupling in svMCI. Specifically, F–S couplings were preserved at the whole brain level but reduced within the ventral and increased within the dorsal attention modules. In addition, decreased intramodular connectivity strength in the visual, somatomotor, and dorsal attention modules and reduced intermodular connectivity strength between several modules in the functional network mainly linking the visual, somatomotor, dorsal attention, ventral attention, and frontoparietal control modules were found. Overall, these findings may provide valuable insights for a better understanding of the pathophysiological mechanisms of svMCI.

Acknowledgements This work was supported by the Natural Science Foundation of Tianjin Municipal Science and Technology Commission (18JCQNJC10900) and Tianjin Natural Science Foundation (17JCZDJC36300). We thank Qingqing Yang, Dan Zhu, Minghui Hua, Yang Zhang, and Yujuan Cao for their helpful advice on this work.

Conflict of interest The authors claim that they have no conflict of interest.

References

- O'Brien JT, Erkinjuntti T, Reisberg B, Roman G, Sawada T, Pantoni L, *et al.* Vascular cognitive impairment. *Lancet Neurol* 2003, 2: 89–98.
- Moorhouse P, Rockwood K. Vascular cognitive impairment: current concepts and clinical developments. *Lancet Neurol* 2008, 7: 246–255.
- Bu XL, Li WW, Wang YJ. Is Alzheimer's Disease Transmissible in Humans? *Neurosci Bull* 2019, 35: 1113–1115.
- Frisoni GB, Galluzzi S, Bresciani L, Zanetti O, Geroldi C. Mild cognitive impairment with subcortical vascular features: clinical characteristics and outcome. *J Neurol* 2002, 249: 1423–1432.
- Lyu H, Wang J, Xu J, Zheng H, Yang X, Lin S, *et al.* Structural and functional disruptions in subcortical vascular mild cognitive impairment with and without depressive symptoms. *Front Aging Neurosci* 2019, 11: 241.
- Jak AJ, Bondi MW, Delano-Wood L, Wierenga C, Corey-Bloom J, Salmon DP, *et al.* Quantification of five neuropsychological approaches to defining mild cognitive impairment. *Am J Geriatr Psychiatry* 2009, 17: 368–375.
- Ravaglia G, Forti P, Maioli F, Martelli M, Servadei L, Brunetti N, *et al.* Conversion of mild cognitive impairment to dementia:

- predictive role of mild cognitive impairment subtypes and vascular risk factors. *Dement Geriatr Cogn Disord* 2006, 21: 51–58.
8. Seo SW, Ahn J, Yoon U, Im K, Lee JM, Tae Kim S, *et al.* Cortical thinning in vascular mild cognitive impairment and vascular dementia of subcortical type. *J Neuroimaging* 2010, 20: 37–45.
 9. Kim SH, Park JS, Ahn HJ, Seo SW, Lee JM, Kim ST, *et al.* Voxel-based analysis of diffusion tensor imaging in patients with subcortical vascular cognitive impairment: correlates with cognitive and motor deficits. *J Neuroimaging* 2011, 21: 317–324.
 10. Dennis EL, Thompson PM. Functional brain connectivity using fMRI in aging and Alzheimer's disease. *Neuropsychol Rev* 2014, 24: 49–62.
 11. Wang J, Zhang Y, Zhu D, Yang Z, Liu F, Qin W, *et al.* A common variant in OXTR rs53576 impacts topological patterns of brain functional networks. *Eur Child Adolesc Psychiatry* 2019.
 12. Liu F, Zhuo C, Yu C. Altered Cerebral Blood Flow Covariance Network in Schizophrenia. *Front Neurosci* 2016, 10: 308.
 13. Xiao F, Lu C, Zhao D, Zou Q, Xu L, Li J, *et al.* Independent component analysis and graph theoretical analysis in patients with narcolepsy. *Neurosci Bull* 2019, 35: 743–755.
 14. Yu Y, Zhou X, Wang H, Hu X, Zhu X, Xu L, *et al.* Small-world brain network and dynamic functional distribution in patients with subcortical vascular cognitive impairment. *PLoS One* 2015, 10: e0131893.
 15. Yi LY, Liang X, Liu DM, Sun B, Ying S, Yang DB, *et al.* Disrupted topological organization of resting-state functional brain network in subcortical vascular mild cognitive impairment. *CNS Neurosci Ther* 2015, 21: 846–854.
 16. Jang YK, Kwon H, Kim YJ, Jung NY, Lee JS, Lee J, *et al.* Early- vs late-onset subcortical vascular cognitive impairment. *Neurology* 2016, 86: 527–534.
 17. Sang L, Chen L, Wang L, Zhang J, Zhang Y, Li P, *et al.* Progressively disrupted brain functional connectivity network in subcortical ischemic vascular cognitive impairment patients. *Front Neurol* 2018, 9: 94.
 18. Zhang Z, Liao W, Chen H, Mantini D, Ding JR, Xu Q, *et al.* Altered functional-structural coupling of large-scale brain networks in idiopathic generalized epilepsy. *Brain* 2011, 134: 2912–2928.
 19. Honey CJ, Sporns O, Cammoun L, Gigandet X, Thiran JP, Meuli R, *et al.* Predicting human resting-state functional connectivity from structural connectivity. *Proc Natl Acad Sci U S A* 2009, 106: 2035–2040.
 20. Hagmann P, Sporns O, Madan N, Cammoun L, Pienaar R, Wedeen VJ, *et al.* White matter maturation reshapes structural connectivity in the late developing human brain. *Proc Natl Acad Sci U S A* 2010, 107: 19067–19072.
 21. Guerra-Carrillo B, Mackey AP, Bunge SA. Resting-state fMRI: a window into human brain plasticity. *Neuroscientist* 2014, 20: 522–533.
 22. Wang Z, Dai Z, Gong G, Zhou C, He Y. Understanding structural-functional relationships in the human brain: a large-scale network perspective. *Neuroscientist* 2015, 21: 290–305.
 23. Skudlarski P, Jagannathan K, Anderson K, Stevens MC, Calhoun VD, Skudlarska BA, *et al.* Brain connectivity is not only lower but different in schizophrenia: a combined anatomical and functional approach. *Biol Psychiatry* 2010, 68: 61–69.
 24. Ding JR, An D, Liao W, Li J, Wu GR, Xu Q, *et al.* Altered functional and structural connectivity networks in psychogenic non-epileptic seizures. *PLoS One* 2013, 8: e63850.
 25. Cocchi L, Harding IH, Lord A, Pantelis C, Yucel M, Zalesky A. Disruption of structure-function coupling in the schizophrenia connectome. *Neuroimage Clin* 2014, 4: 779–787.
 26. Kim DJ, Schnakenberg Martin AM, Shin YW, Jo HJ, Cheng H, Newman SD, *et al.* Aberrant structural-functional coupling in adult cannabis users. *Hum Brain Mapp* 2019, 40: 252–261.
 27. Sporns O. Network attributes for segregation and integration in the human brain. *Curr Opin Neurobiol* 2013, 23: 162–171.
 28. Park HJ, Friston K. Structural and functional brain networks: from connections to cognition. *Science* 2013, 342: 1238411.
 29. Sporns O, Tononi G, Edelman GM. Theoretical neuroanatomy: relating anatomical and functional connectivity in graphs and cortical connection matrices. *Cereb Cortex* 2000, 10: 127–141.
 30. Kotter R, Stephan KE. Network participation indices: characterizing component roles for information processing in neural networks. *Neural Netw* 2003, 16: 1261–1275.
 31. Latora V, Marchiori M. Efficient behavior of small-world networks. *Phys Rev Lett* 2001, 87: 198701.
 32. Han JD, Bertin N, Hao T, Goldberg DS, Berriz GF, Zhang LV, *et al.* Evidence for dynamically organized modularity in the yeast protein-protein interaction network. *Nature* 2004, 430: 88–93.
 33. Sporns O, Honey CJ, Kotter R. Identification and classification of hubs in brain networks. *PLoS One* 2007, 2: e1049.
 34. He Y, Wang J, Wang L, Chen ZJ, Yan C, Yang H, *et al.* Uncovering intrinsic modular organization of spontaneous brain activity in humans. *PLoS One* 2009, 4: e5226.
 35. Seo SW, Cho SS, Park A, Chin J, Na DL. Subcortical vascular versus amnesic mild cognitive impairment: comparison of cerebral glucose metabolism. *J Neuroimaging* 2009, 19: 213–219.
 36. Galluzzi S, Sheu CF, Zanetti O, Frisoni GB. Distinctive clinical features of mild cognitive impairment with subcortical cerebrovascular disease. *Dement Geriatr Cogn Disord* 2005, 19: 196–203.
 37. Lawrence AJ, Chung AW, Morris RG, Markus HS, Barrick TR. Structural network efficiency is associated with cognitive impairment in small-vessel disease. *Neurology* 2014, 83: 304–311.
 38. Dichgans M, Leys D. Vascular Cognitive Impairment. *Circ Res* 2017, 120: 573–591.
 39. Schaefer A, Kong R, Gordon EM, Laumann TO, Zuo XN, Holmes AJ, *et al.* Local-global parcellation of the human cerebral cortex from intrinsic functional connectivity MRI. *Cereb Cortex* 2018, 28: 3095–3114.
 40. Sha Z, Versace A, Edmiston EK, Fournier J, Graur S, Greenberg T, *et al.* Functional disruption in prefrontal-striatal network in obsessive-compulsive disorder. *Psychiatry Res Neuroimaging* 2020, 300: 111081.
 41. Yeo BT, Krienen FM, Sepulcre J, Sabuncu MR, Lashkari D, Hollinshead M, *et al.* The organization of the human cerebral cortex estimated by intrinsic functional connectivity. *J Neurophysiol* 2011, 106: 1125–1165.
 42. Achard S, Bullmore E. Efficiency and cost of economical brain functional networks. *PLoS Comput Biol* 2007, 3: e17.
 43. Liu F, Guo W, Fouche JP, Wang Y, Wang W, Ding J, *et al.* Multivariate classification of social anxiety disorder using whole brain functional connectivity. *Brain Struct Funct* 2015, 220: 101–115.
 44. Wang J, Wang X, He Y, Yu X, Wang H, He Y. Apolipoprotein E epsilon4 modulates functional brain connectome in Alzheimer's disease. *Hum Brain Mapp* 2015, 36: 1828–1846.
 45. Fox MD, Zhang D, Snyder AZ, Raichle ME. The global signal and observed anticorrelated resting state brain networks. *J Neurophysiol* 2009, 101: 3270–3283.
 46. Murphy K, Birn RM, Handwerker DA, Jones TB, Bandettini PA. The impact of global signal regression on resting state correlations: are anti-correlated networks introduced? *Neuroimage* 2009, 44: 893–905.
 47. Weissenbacher A, Kasess C, Gerstl F, Lanzenberger R, Moser E, Windischberger C. Correlations and anticorrelations in resting-

- state functional connectivity MRI: a quantitative comparison of preprocessing strategies. *Neuroimage* 2009, 47: 1408–1416.
48. Mori S, Crain BJ, Chacko VP, van Zijl PC. Three-dimensional tracking of axonal projections in the brain by magnetic resonance imaging. *Ann Neurol* 1999, 45: 265–269.
 49. Sun Y, Dai Z, Li J, Collinson SL, Sim K. Modular-level alterations of structure-function coupling in schizophrenia connectome. *Hum Brain Mapp* 2017, 38: 2008–2025.
 50. Thottakara P, Lazar M, Johnson SC, Alexander AL. Application of Brodmann's area templates for ROI selection in white matter tractography studies. *Neuroimage* 2006, 29: 868–878.
 51. Li Y, Liu Y, Li J, Qin W, Li K, Yu C, *et al.* Brain anatomical network and intelligence. *PLoS Comput Biol* 2009, 5: e1000395.
 52. Gong G, He Y, Concha L, Lebel C, Gross DW, Evans AC, *et al.* Mapping anatomical connectivity patterns of human cerebral cortex using in vivo diffusion tensor imaging tractography. *Cereb Cortex* 2009, 19: 524–536.
 53. Lo CY, Wang PN, Chou KH, Wang J, He Y, Lin CP. Diffusion tensor tractography reveals abnormal topological organization in structural cortical networks in Alzheimer's disease. *J Neurosci* 2010, 30: 16876–16885.
 54. Buchanan CR, Pernet CR, Gorgolewski KJ, Storkey AJ, Bastin ME. Test-retest reliability of structural brain networks from diffusion MRI. *Neuroimage* 2014, 86: 231–243.
 55. Bassett DS, Bullmore E, Verchinski BA, Mattay VS, Weinberger DR, Meyer-Lindenberg A. Hierarchical organization of human cortical networks in health and schizophrenia. *J Neurosci* 2008, 28: 9239–9248.
 56. He Y, Chen Z, Evans A. Structural insights into aberrant topological patterns of large-scale cortical networks in Alzheimer's disease. *J Neurosci* 2008, 28: 4756–4766.
 57. Collin G, Scholtens LH, Kahn RS, Hillegers MHJ, van den Heuvel MP. Affected anatomical rich club and structural-functional coupling in young offspring of schizophrenia and bipolar disorder patients. *Biol Psychiatry* 2017, 82: 746–755.
 58. Fukushima M, Betzel RF, He Y, van den Heuvel MP, Zuo XN, Sporns O. Structure-function relationships during segregated and integrated network states of human brain functional connectivity. *Brain Struct Funct* 2018, 223: 1091–1106.
 59. Baum GL, Cui Z, Roalf DR, Ciric R, Betzel RF, Larsen B, *et al.* Development of structure-function coupling in human brain networks during youth. *Proc Natl Acad Sci U S A* 2020, 117: 771–778.
 60. Honey CJ, Thivierge JP, Sporns O. Can structure predict function in the human brain? *Neuroimage* 2010, 52: 766–776.
 61. Fox MD, Corbetta M, Snyder AZ, Vincent JL, Raichle ME. Spontaneous neuronal activity distinguishes human dorsal and ventral attention systems. *Proc Natl Acad Sci U S A* 2006, 103: 10046–10051.
 62. Barrett AM, Boukrina O, Saleh S. Ventral attention and motor network connectivity is relevant to functional impairment in spatial neglect after right brain stroke. *Brain Cogn* 2019, 129: 16–24.
 63. Lim JS, Kang DW. Stroke Connectome and Its Implications for Cognitive and Behavioral Sequela of Stroke. *J Stroke* 2015, 17: 256–267.
 64. Li C, Zheng J, Wang J. An fMRI study of prefrontal cortical function in subcortical ischemic vascular cognitive impairment. *Am J Alzheimers Dis Other Dement* 2012, 27: 490–495.
 65. Hutchison RM, Womelsdorf T, Allen EA, Bandettini PA, Calhoun VD, Corbetta M, *et al.* Dynamic functional connectivity: promise, issues, and interpretations. *Neuroimage* 2013, 80: 360–378.
 66. Liu F, Wang Y, Li M, Wang W, Li R, Zhang Z, *et al.* Dynamic functional network connectivity in idiopathic generalized epilepsy with generalized tonic-clonic seizure. *Hum Brain Mapp* 2017, 38: 957–973.
 67. Bi K, Hua L, Wei M, Qin J, Lu Q, Yao Z. Dynamic functional-structural coupling within acute functional state change phases: Evidence from a depression recognition study. *J Affect Disord* 2016, 191: 145–155.
 68. Zalesky A, Fornito A, Harding IH, Cocchi L, Yucel M, Pantelis C, *et al.* Whole-brain anatomical networks: does the choice of nodes matter? *Neuroimage* 2010, 50: 970–983.
 69. Wang J, Wang L, Zang Y, Yang H, Tang H, Gong Q, *et al.* Parcellation-dependent small-world brain functional networks: a resting-state fMRI study. *Hum Brain Mapp* 2009, 30: 1511–1523.
 70. Gordon EM, Laumann TO, Gilmore AW, Newbold DJ, Greene DJ, Berg JJ, *et al.* Precision functional mapping of individual human brains. *Neuron* 2017, 95: 791–807. e797.
 71. Mueller S, Wang D, Fox MD, Yeo BT, Sepulcre J, Sabuncu MR, *et al.* Individual variability in functional connectivity architecture of the human brain. *Neuron* 2013, 77: 586–595.
 72. Wang D, Buckner RL, Fox MD, Holt DJ, Holmes AJ, Stoecklein S, *et al.* Parcellating cortical functional networks in individuals. *Nat Neurosci* 2015, 18: 1853–1860.
 73. Laumann TO, Gordon EM, Adeyemo B, Snyder AZ, Joo SJ, Chen MY, *et al.* Functional system and areal organization of a highly sampled individual human brain. *Neuron* 2015, 87: 657–670.
 74. Suarez LE, Markello RD, Betzel RF, Misic B. Linking structure and function in macroscale brain networks. *Trends Cogn Sci* 2020, 24: 302–315.